Trans. JSASS Aerospace Tech. Japan
Vol. 17, No. 5, pp. 561-567, 2019
DOI: 10.2322/tastj. 17. 561

Temperature Estimations of SiC Ablations with Several Kinds of Narrow Band-pass Filters*

By Makoto HASHIMOTO,[1)] Masato FUNATSU,[1)] Nurul MALISA,[2)] Gen MORIOKA,[3)] and Masahiro OZAWA[4)]

[1)]*Graduate School of Science and Technology, Gunma University, Kiryu, Japan*
[2)]*Tateyama Auto Machine Co., (M) Sdn., Bhd., Shah Alam, Malaysia*
[3)]*Mitsubishi Electric Engineering Co., Ltd., Kamakura, Japan*
[4)]*Chuo Engineering Co., Ltd., Tokyo, Japan*

(Received October 3rd, 2017)

When a spacecraft reenters the Earth's atmosphere, it becomes overheated by the strong shock waves generated ahead of the vehicle. To protect the vehicle from severe aerodynamic heating, one can apply a thermal protection system using a technique known as the ablation method. However, the properties and behavior of ablation remain poorly understood, necessitating further research. The present study conducts ablation experiments on silicon carbide using two kinds of narrow band-pass filters with different measuring wavelengths. During the ablation, the radiation intensity distribution was calculated from the spontaneous emission images of the test piece acquired through each filter. Based on the relationship between the radiation intensity distribution ratio and temperature, the estimated surface temperature of the test piece after 10 s of heating ranged from 1,800 K at the rear to 3,000 K at the tip.

Key Words: Temperature Estimation, Silicon Carbide, Ablation, Plasma Freejet, Plasma Diagnosis

Nomenclature

A	:	sectional area of the calorimeter
C_p	:	specific heat at constant pressure of water
f	:	flow rate of water
q	:	heat flux value
ΔT	:	temperature difference of water
ρ_w	:	density of water

1. Introduction

When a spacecraft reenters the Earth's atmosphere, it undergoes severe aerodynamic heating owing to the strong shock waves generated ahead of the vehicle. The heating rate is especially severe during reentry at super-orbital velocities. For example, the maximum heating rate at the stagnation point of the Hayabusa (MUSES-C) during reentry was 15 MW/m^2.[1)] To prevent such overheating, space vehicles can be thermally treated by the ablation method, which is a thermal protection system for protecting the vehicle from such heat. The heat generated during reentry induces a phase change in the ablative materials. Currently, the surface of the spacecraft is coated by a heat-resistant material (typically a carbon–phenolic composite material). However, these materials are subjected to thermal decomposition and mechanical damage due to the severe heating during reentry into the atmosphere. The wear on the spacecraft renders the vehicle unfit for reuse. Therefore, the coating on the spacecraft must be replaced for each new mission, necessitating repeated and costly production of heat-resistant material. As cost reduction in manufacturing is important for developing the aerospace industry, heat-resistant materials are being actively researched.[2),3)] Accordingly, accurately predicting the wear behavior of heat-resistant materials in high-temperature environments is essential. Indeed, the thermal response of ablation has been investigated since the 1960s.[4)]

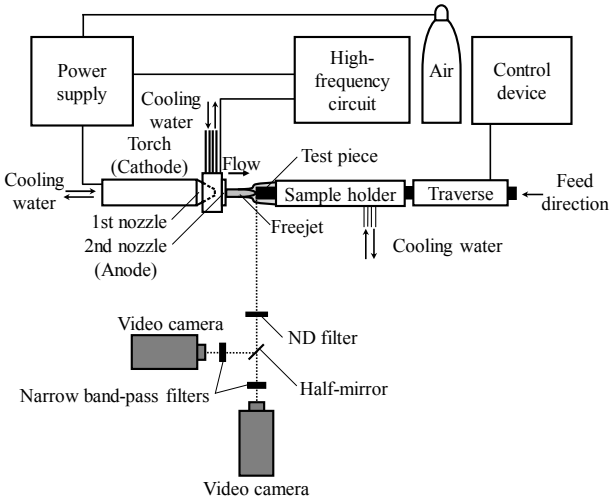

Fig. 1. Schematic of the experimental setup (for radiation measurements).

Silicon carbide (SiC) is recognized as a good heat-resistant material owing to its high density, wear resistance, high thermal conductivity, and oxidation resistance.[5)] Therefore, SiC can absorb and reduce the se-

*Presented at the 31st International Symposium on Space Technology and Science, June 3-9, 2017, Ehime, Japan

vere aerodynamic heating from the high-temperature plasma flows encountered by a spacecraft during reentry.[5] However, although the use of SiC is expected to occur in the manufacturing of spacecraft, the properties and behavior of SiC ablations remain unclarified, and further research is thus important.[5-8]

Our laboratory conducts systematic ablation experiments on SiC using air plasma freejets.[9-12] The final goal is to evaluate the behavior of SiC ablation by measuring the radiation at the surface of the test piece and the gas generated around the test piece in simultaneous multi-wavelength measurements. As a first step, we established a two-wavelength simultaneous measurement method and estimated the temperature of the test piece surface.

The two-wavelength simultaneous measurement method is also adopted in other disciplines besides the space business, but our laboratory is the first to apply this temperature estimation method to SiC ablation. Our laboratory replaces the pyrometer point measurements in the standard two-wavelength simultaneous measurement method[13] with surface measurements. In this approach, the surface temperature over the entire test piece can be estimated from images of the radiative intensity distribution. However, the method requires two narrow band-pass filters that correspond to the temperatures measured. The theoretical curve of Planck's law of radiation must also be considered.

In previous research,[12] spectroscopic measurements of the radiation of SiC ablation were performed at three representative points. The resulting spectrum acquired from the test piece was then fitted with the radiation intensity distribution. At 20 s after the start of heating (to allow the test-piece shape to stabilize), the radiation from the test-piece surface was acquired using two kinds of narrow band-pass filters and two general-purpose video cameras. From the intensity ratio calculated and the theoretical intensity curve, the apparent temperature of the SiC was estimated after the start of heating.

The present research performs radiation measurements of SiC ablation using narrow band-pass filters and general-purpose video cameras. As in our previous research, the test-piece surface was irradiated after 20 s of heating to allow the shape to settle, and its apparent temperature was estimated from the intensity ratio calculated and the theoretical intensity curve. In addition, the changing shape of the test piece and the temperature distribution estimated over an elapsed time of 30 s after the start of heating were analyzed in detail.

2. Experimental Setup and Method

Figure 1 is a schematic of the experimental setup used for radiation measurements. The experimental setup is divided into two main sections: a plasma freejet generator section and an observation section. The former section is comprised of a plasma freejet generating device, a sample holder and an automatic feeding device. Figure 2 is a schematic of the plasma freejet generator nozzle layout.[10]

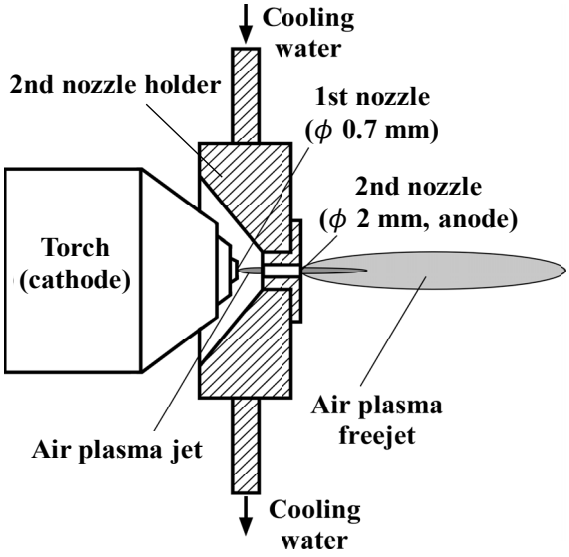

Fig. 2. Schematic of the plasma freejet generator nozzle layout.[10]

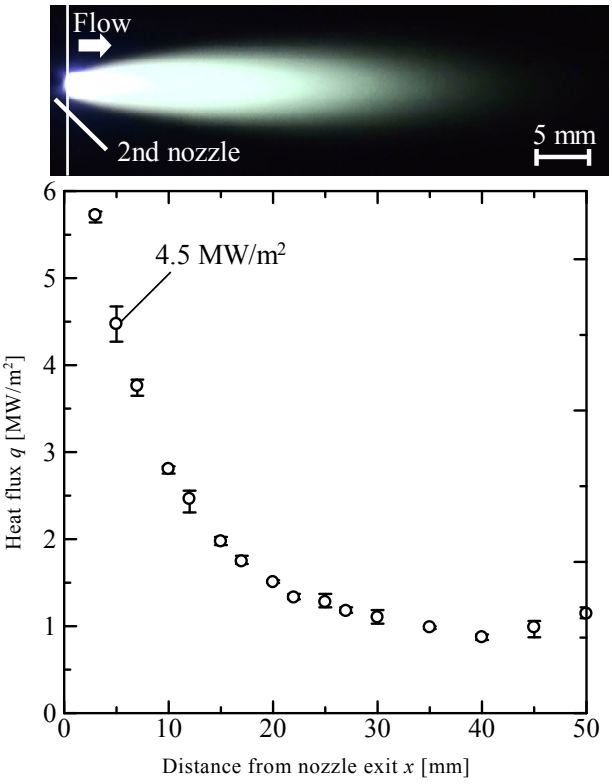

Fig. 3. Photograph of the plasma emission[11] and heat flux distribution along the flow axis[10] of the air plasma freejets.

Fig. 4. Silicon-carbide sample used in the experiment (SiC, diameter 2.0 mm).

The generator torch is comprised of a cathode integrated with the first (1st) nozzle, which has an outer diameter of 0.7 mm. The second (2nd) nozzle is installed outside the torch and acts as an anode. The working gas is atmospheric air (volume ratio; N_2:O_2 = 79:21). The 1st and 2nd nozzles are separated by a 3.0 mm space. Microscopic air plasma jets are generated and jetted from the exit of the 2nd nozzle, creating air plasma freejets. The 2nd nozzle holder is cooled by water flowing.

The upper panel of Fig. 3 is a video image of the air plasma freejet.[11] The air plasma freejet was emitted from the exit of the 2nd nozzle, and extended to approximately 40 mm in the horizontal direction. The freejet was initially white, turning to pale-green at its endpoint. To generate the air plasma freejet, the discharge current was set to 10 A, the discharge voltage was 180.0–185.0 V, and the reservoir and atmospheric pressures were 0.6 MPa (absolute pressure) and 0.1 MPa (atmospheric pressure), respectively. The sample holder has a triple-circular tube structure and is cooled by means of an internal water flow. The tip of the test piece was set 5.0 mm from the exit of the 2nd nozzle on the central axis of the air plasma freejet. The lower panel of Fig. 3 plots the heat flux as a function of distance from the nozzle exit.[7] The heat fluxes were measured using a calorimeter installed in the flow direction of the air plasma freejets. From the calorimeter measurements, the heat flux was calculated by Eq. (1):

$$q = \rho_w C_p f \Delta T / A. \quad (1)$$

As shown in the figure, the heat flux decreased as the distance from the exit of the 2nd nozzle increased. Heat flux decreased rapidly up to approximately 20 mm from the exit and became almost constant thereafter. Both panels in Fig. 3 show that the heat flux was relatively large in the initial white emission region, but relatively small in the pale-green emission region of the freejet. The ablation experiments are conducted at 5.0 mm from the exit of the 2nd nozzle, where the heating ratio is high. The heat flux at this position is 4.5 MW/m^2. As the position of the tip of the test piece recedes throughout the ablation process, the test piece moves at a constant speed (0.61 mm/s) using an automatic feeding device. Figure 4 presents the test piece used in this research. The test piece was a round SiC bar with a cross-sectional diameter of 2.0 mm. In the radiation measurements, the radiation emissions of the SiC ablations are divided into two light paths using a half-mirror, and the radiations at two specific wavelengths are simultaneously captured using two general-purpose video cameras (Sony HDR-XR550V and HDR-CX720V). The pixel numbers of the XR550V and CX720V cameras are 4,150,000 and 6,140,000, respectively.

3. Experimental Results and Discussion

3.1. Spectroscopic measurements of SiC ablations

For spectroscopic measurements, the radiation of the SiC ablation is focused onto the fiber of the spectrometer through a quartz lens. Figure 5 shows a video image captured during the SiC ablation experiment. As the radiation during the ablation process was remarkably strong, the image was taken through neutral density (ND) filters (Sigmakoki Co., Ltd.) (optical density = 3.0) with an attenuation ratio of 1/10^3. The condition of the test piece during the ablation is difficult to discern because the radiation around it is stronger than the emission of the test piece itself. However, a strong emission is observed at the tip of the test piece. This emission was found to spread radially toward the rear of the test piece. The pale-green region at the rear of the test piece is attributable to the gas escaping from the SiC. The spectroscopic measurements were performed at the red point on the test piece, as

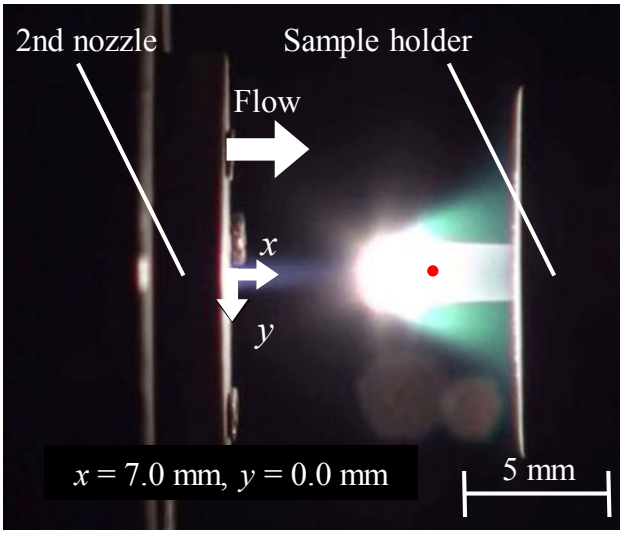

Fig. 5. Measurement points for spectroscopic measurements (O.D. = 3.0).

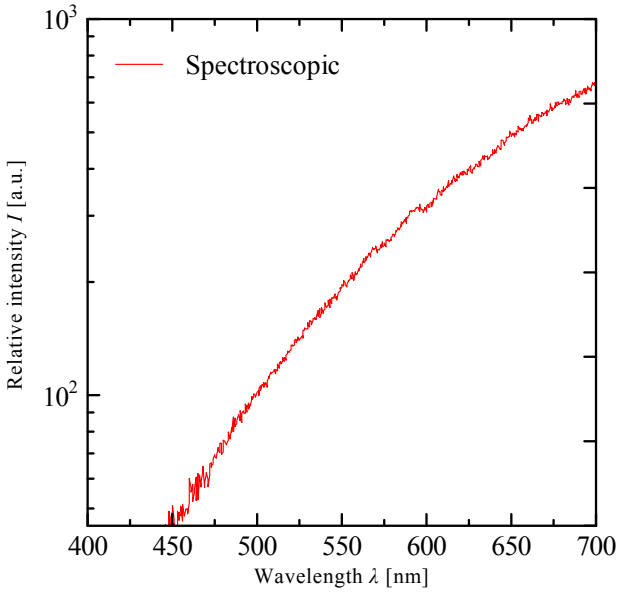

Fig. 6. Spectrum of SiC ablations.[12]

shown in the image. The measurement results (relative intensity versus wavelength) are displayed in Fig. 6.[12] The spectrum became continuous at wavelengths exceeding 450 nm. In previous research,[12] the continuous spectrum recorded was fitted by Planck's law of radiation and the temperature of the test piece was estimated. To validate the method, the results from fitting by Planck's law of radiation were compared with the results derived through pyrometer measurements. The temperatures obtained by the two methods differed by 50 K, within the error margin determined in an error analysis of the pyrometer values. Hence, this value is considered within the range of error, and Planck's law of radiation is deemed suitable for estimating the apparent surface temperatures of SiC ablations in this study.

3.2. Radiation measurements of SiC ablations

Radiation from the SiC ablations was passed through two kinds of narrow band-pass filters and measured simultaneously using two general-purpose video cameras. The narrow band-pass filters were MC520 and MC650 (Asahi Spectra Co., Ltd.) with filter wavelengths of 520 nm and 650 nm, respectively. Figure 6 shows the continuous spectrum obtained in the filtered wavelength region,[12] and Table 1 shows the characteristics of the narrow band-pass filters. The strong radiation of the SiC ablations was attenuated through a ND filter (O.D. = 5.0). The video cameras were operated under the following shutter conditions: shutter speed = 60 frames/s, exposure time = 250 μs. Figure 7 is a pseudo color display of the radiation intensity distributions acquired by the video cameras. The color depends on the wavelength sensitivity and transmittance of the narrow band-pass filters. The upper and lower images were acquired through the MC520 and MC650 filters, respectively. The images in Fig. 7 were taken at different elapsed times after the start of heating. The identity of each frame was secured by setting both cameras at the same shutter speed and same position. The moment the air plasma freejet occurred was considered to be 0 s. The left and right vertical white lines in the images indicate the exit of the 2nd nozzle and the position of the sample holder, respectively. The color bar beneath the images indicates the relative intensity of the radiation emitted. The images confirm that the radiation intensity was stronger after MC650 filtering than that after MC520 filtering. In addition, the radiation intensity was weaker in the peripheral part than at the inner side of the test piece (although this phenomenon is difficult to distinguish). The test-piece surface is considered to be the region of continuous phase change on the test piece, where the chemical species related to C and Si were irradiated. The radiation intensity at the tip of the test piece was stronger after MC650 filtering than that after MC520 filtering. At 10 s after the start of heating, the tip of the originally cylindrical test piece had tapered. As the shape of the heated surface evolved from a 2.0-mm-diameter cross-section to a blunt point, the air plasma freejet was more easily wrapped around the side of the test piece.

Table 1. Characteristics of the narrow band-pass filters.

Filter Name	Wavelength [nm]	FWHM [nm]	Transmittance [%]
MC520	521.00	10.00	83.0
MC650	648.75	12.50	89.7

3.3. Temperature estimations of SiC ablations

The apparent surface temperatures of SiC ablations were estimated from the radiation intensity ratios of the MC520 and MC650 filters. Specifically, the theoretical radiation intensity ratios at 520 and 650 nm wavelengths were calculated by theoretical Planck's law of radiation at different temperatures, and adapted to the intensity ratio of the radiation measurement results. Figure 8 plots the logarithmic theoretical radiation intensity versus wavelength curves at different temperatures. The black vertical lines indicate the center-wavelength positions of the narrow band-pass filters used in this experiment. The theoretical radiation intensity ratio, determined from the theoretical radiant intensity ratios at different wavelengths (intensity of 650 nm divided by intensity of 520 nm in Fig. 8), is plotted against temperature in Fig. 9. The temperature at which the radiation intensity ratio in Fig. 9 matched the experimentally determined radiation intensity distribution ratio was estimated as the apparent temperature of the test-piece surface. If the intensity ratios of both wavelengths are high, other combinations of narrow band filters should yield the same temperature values at the same times. Figure 10 shows the estimated surface-temperature distribution of the test piece at the instances when the snapshots were clicked, which are the same as those shown in Fig. 7. Here, the color bar represents temperature rather than relative intensity. Based on Fig. 10, the temperatures at the tip and rear of the test piece were approximately 3,000 K and 1,800 K, respectively. Furthermore, the yellow-to-red area (the high-temperature region, ~2,400–3,000 K) increased as the elapsed time increased. This increase reflects the changing shape of the test piece discussed in Section 3.2. As the air plasma freejet wrapped around and heated the side of the test piece, the heated area increased, expanding the high-temperature region of the test-piece surface.

The temperatures estimated by Plank's law of radiation and the single-point spectroscopic measurements of the test piece differed by approximately 200 K.

The temperature-distribution dynamics of SiC ablation were analyzed in visualization experiments of the gas emitted during the ablation process.

4. Conclusion

The radiation emitted by the SiC ablations passed through narrow band-pass filters with different measurement wavelengths and simultaneously imaged using two general-purpose video cameras. In addition, the temperature distribution was estimated at different elapsed times, and the changes were analyzed and considered in detail. The main conclusions are summarized as follows:

(1) The radiation intensity passed through the 650-nm filter was stronger than that passed through the 520-nm filter.

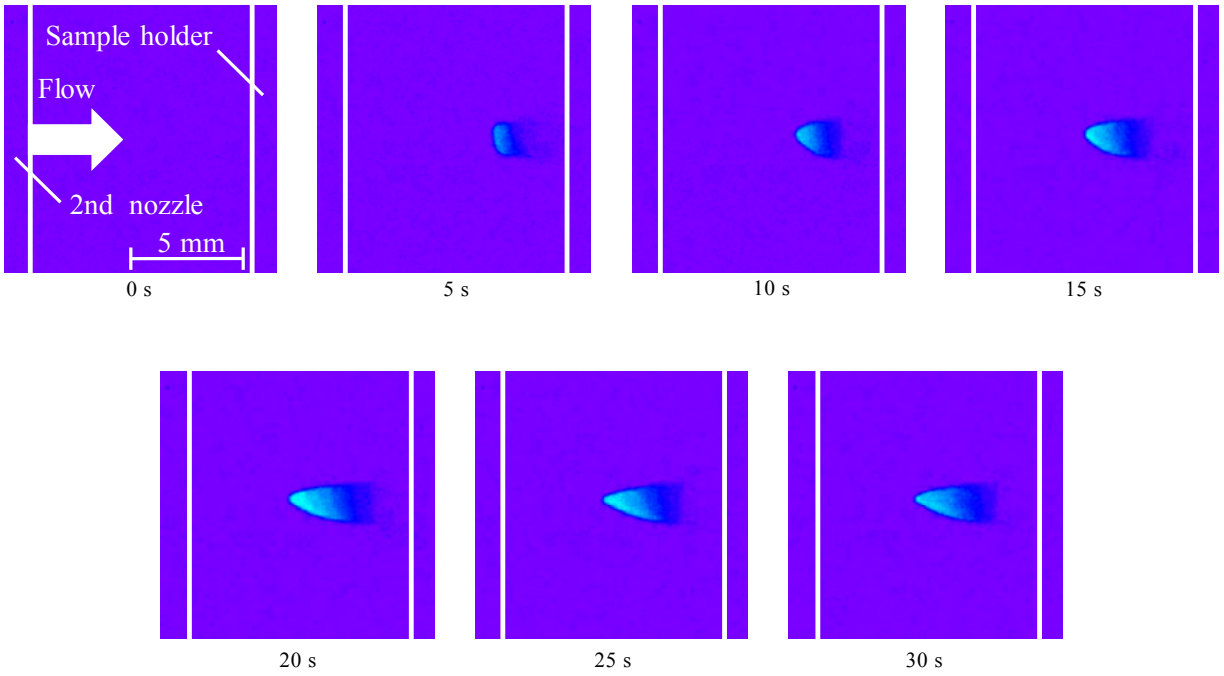

Narrow band-pass filter: MC520 (O.D. = 5.0)

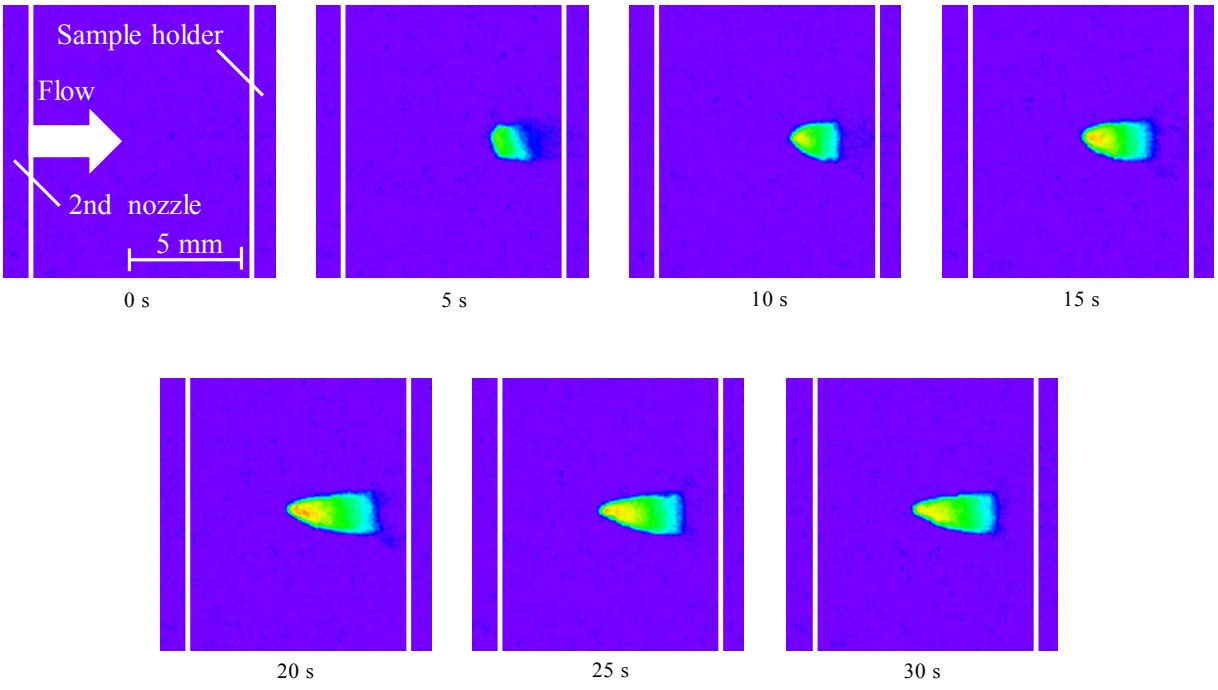

Narrow band-pass filter: MC650 (O.D. = 5.0)

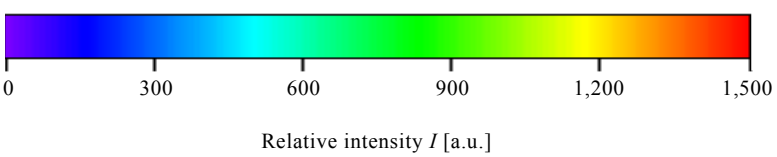

Fig. 7. Video camera images of SiC ablations passed through narrow band-pass filters.

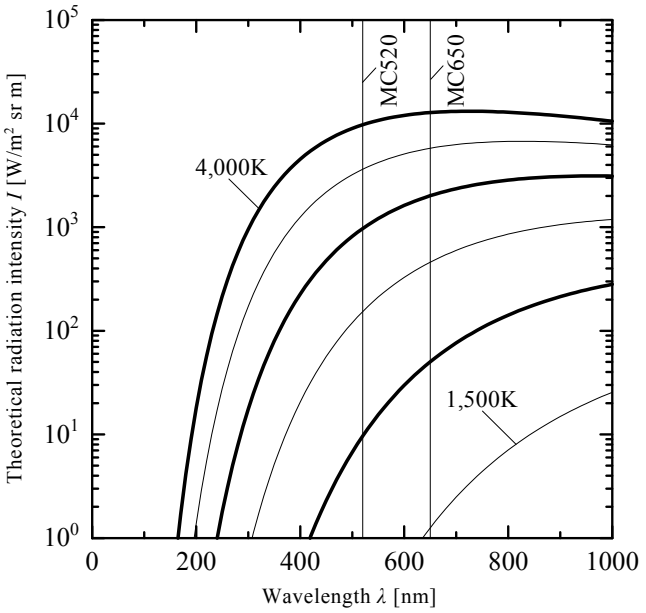

Fig. 8. Relationship between wavelength and theoretical radiation intensity.

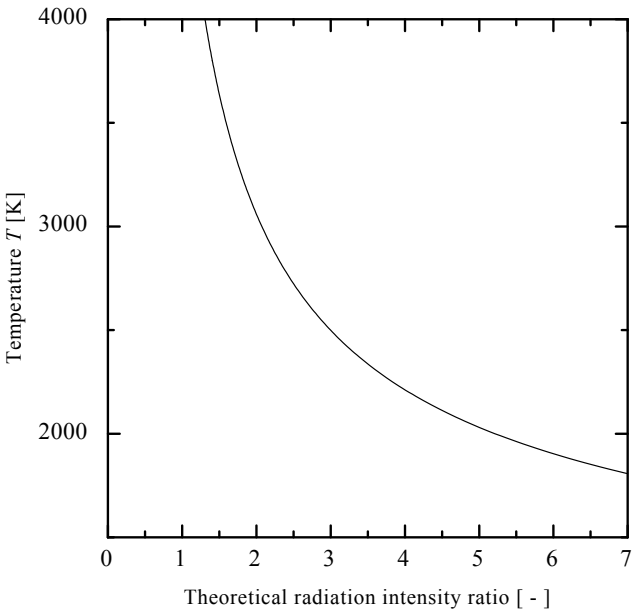

Fig. 9. Relationship between theoretical radiation intensity ratio and temperature.

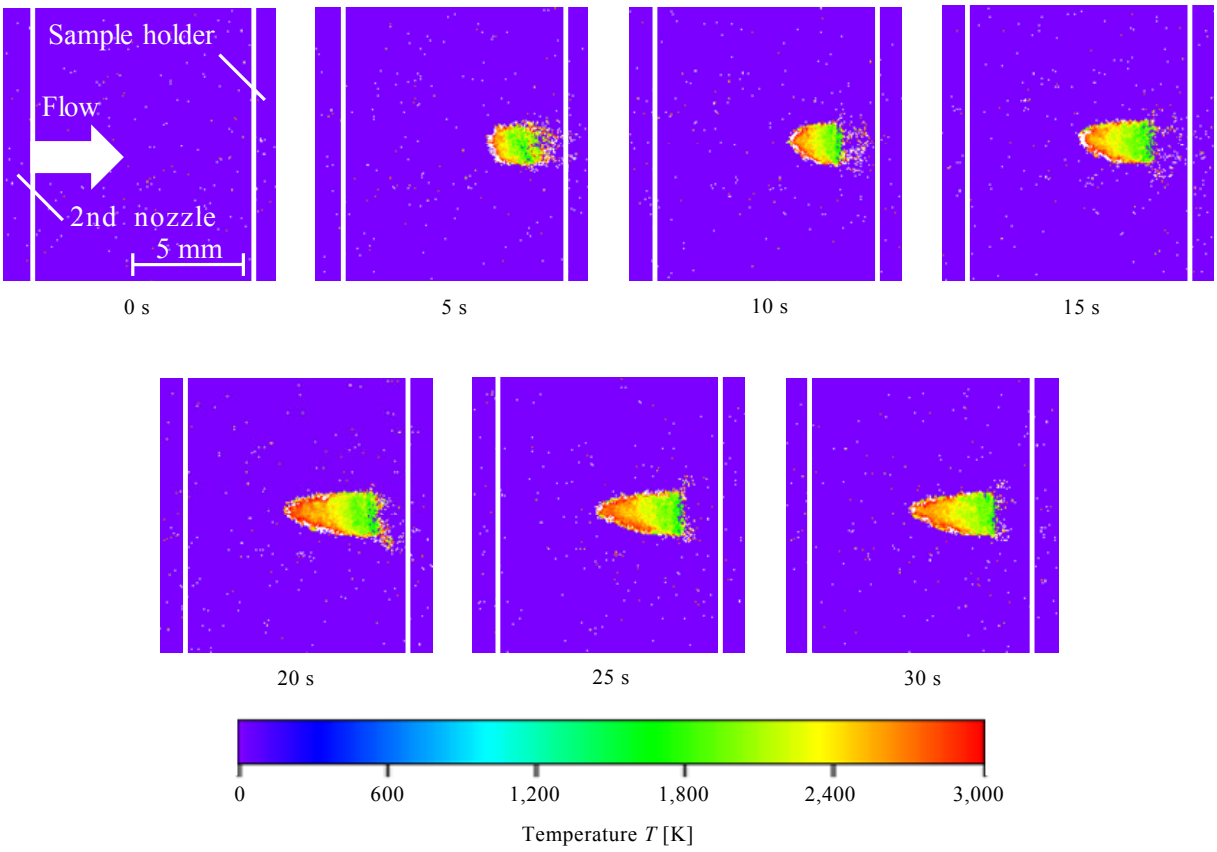

Fig. 10. Temperature estimations of SiC ablations.

(2) At 10 s after the start of heating, the tip shape of the test piece had evolved from a cylindrical cross-section to a tapered blunt point.

(3) The estimated temperatures at the tip and rear of the test piece were approximately 3,000 K and 1,800 K, respectively.

(4) The high-temperature flow around the test piece generated a high-temperature region (2,400–3,000 K). As time elapsed, this region grew from the tip of the test piece.

Acknowledgments

This work was supported partly by JSPS KAKENHI Grant Number JP25420847 and JP17K06941.

References

1) Ishii, N., Yamada, T., Hiraki, K., and Inatani, Y.: Reentry Motion and Aerodynamics of the MUSES-C Sample Return Capsule, *Trans. Jpn. Soc. Aeronaut. Space Sci.*, **51** (2008), pp. 65-70.
2) Ragab, M. M., Cheatwood, F. M., Hughes, S. J., and Lowry, A.: Launch Vehicle Recovery and Reuse, AIAA Paper 2015-4490, 2015.
3) Shuyuan, Z., Boming, Z., and Shanyi, D.: Effects of Contact Resistance on Heat Transfer Behaviors of Fibrous Insulation, *Chinese J. Aeronautics*, **22** (2009), pp. 569-574.
4) Prakash, A. and Zhong, X.: Numerical Simulation of Planetary Reentry Aeroheating over Blunt Bodies with Non-equilibrium Reacting Flow, AIAA Paper 2008-744, 2008.
5) Tran, H. K. and Sawko, P. M.: Thermal Degradation Study of Silicon Carbide Threads Developed for Advanced Flexible Thermal Protection Systems, NASA-TM-103952, 1992.
6) Metzger, J. W., Engel, M. J., and Diaconis, N. S.: Oxidation and Sublimation of Graphite in Simulated Re-Entry Environments, *AIAA J.*, **5** (1967), pp. 451-460.
7) Park, C.: Review of Chemical-Kinetic Problems of Future NASA Missions, I: Earth Entries, *J. Thermophysics and Heat Transfer*, **7** (1993), pp. 385-398.
8) Milos, F. S.: Galileo Probe Heat Shield Ablation Experiment, *J. Spacecraft and Rockets*, **34** (1997), pp. 705-713.
9) Funatsu, M., Kasuya, K., and Shirai, H.: Radiative Characteristics of Carbonaceous Ablation Layers with Reflection Effects, *JSME International J. Series B, Fluids and Thermal Engineering*, **44** (2001), pp. 419-426.
10) Funatsu, M., Ozawa, M., Shirai, H., and Takakusagi, F.: Experimental Study of Ablation Processes of SiC-based Materials in Air Plasma Freejets, *Trans. JSASS Aerospace Tech. Japan,* **8**, ists27 (2010), pp. Pe_41-Pe_46.
11) Ozawa, M., Funatsu, M., Onozawa, R., Shibata, R., Shirai, H., and Takakusagi, F.: Spectroscopic Measurements of SiC Ablations in Air Plasma Freejets, *Trans. JSASS Aerospace Tech. Japan,* **10**, ists28 (2012), pp. Pe_41-Pe_47.
12) Morioka, G., Tokano, K., Konishi, K., Ozawa, M., and Funatsu, M.: Radiation Measurements of SiC Ablations with Several Kinds of Narrow Band-pass Filters, 30th International Symposium on Space Technology and Science, Kobe, Japan, 2015-e-33, 2015.
13) Kato, S., Okuyama, K., Nishio, S., Sakata, R., Hama, K., and Inatani, Y.: Numerical Analysis of Charring Ablation for Ablative Materials of Re-Entry Capsules, *J. Jpn. Soc. Aeronaut. Space Sci.*, **50** (2002), pp. 255-263 (in Japanese).